

This item is the archived peer-reviewed author-version of:

A new alkaloid from *Pancreatum maritimum* : structure elucidation using computer-assisted structure elucidation (CASE) and evaluation of cytotoxicity and anti-SARS-CoV-2 activity

Reference:

Le Hien T.N., De Jonghe Steven, Erven Kristien, Neyts Johan, Pannecouque Christophe, Vermeyen Tom, Herrebout Wouter, Pieters Luc, Tuentner Emmy.- A new alkaloid from *Pancreatum maritimum* : structure elucidation using computer-assisted structure elucidation (CASE) and evaluation of cytotoxicity and anti-SARS-CoV-2 activity
Phytochemistry letters - ISSN 1876-7486 - 58(2023), p. 1-7
Full text (Publisher's DOI): <https://doi.org/10.1016/J.PHYTOL.2023.09.006>
To cite this reference: <https://hdl.handle.net/10067/1993800151162165141>

A new alkaloid from *Pancratium maritimum* - Structure elucidation using computer-assisted structure elucidation (CASE) and evaluation of anti-SARS-CoV-2 activity

Ngoc-Thao-Hien Le^{1}, Steven De Jonghe², Kristien Erven², Johan Neyts², Christophe Pannecouque², Tom Vermeyen^{3,4}, Wouter A. Herrebout³, Luc Pieters¹, Emmy Tuentjer¹*

¹Natural Products & Food Research and Analysis (NatuRA), Department of Pharmaceutical Sciences, University of Antwerp, Antwerp, Belgium

²KU Leuven, Department of Microbiology, Immunology and Transplantation, Rega Institute for Medical Research, Laboratory of Virology and Chemotherapy, Leuven, Belgium

³Molecular Spectroscopy (MolSpec), Department of Chemistry, University of Antwerp, Belgium

⁴Ghent Quantum Chemistry Group, Department of Chemistry, Ghent University, Ghent, Belgium

*lengocthaohien@gmail.com or NgocThaoHien.Le@uantwerpen.be

Abstract

Pancratium maritimum L. (or ‘sea daffodil’) is one of the most studied plant species in the Amaryllidaceae family. Recently, due to the advancement of new probabilistic methods and spectroscopic techniques, the potential for phytochemical investigations on isomeric compounds has significantly improved. In this study, application of these techniques in combination with conventional phytochemical analysis led to the isolation and identification of a new alkaloid named 2 β ,10 β -dihydroxy-9-*O*-demethylhomolycorine from *P. maritimum*, together with 17 known ones. Assessment of anti-SARS-CoV-2 activity and cytotoxicity on a Vero E6 cell line for all compounds revealed four compounds with weak anti-SARS-CoV-2 potency at non-cytotoxic concentrations, namely of 9-*O*-demethylhomolycorine (EC₅₀ = 44 μ M), galanthamine (EC₅₀ = 70 μ M), 1-*O*-acetyl-norpluviine (EC₅₀ = 80 μ M) and 1-*O*-acetyl-10-*O*-methylpseudolycorine (EC₅₀ = 47 μ M). On the other hand, cytotoxicity was observed for 2 β ,10 β -dihydroxy-9-*O*-demethylhomolycorine (CC₅₀ = 13.28 μ M), haemanthamine (CC₅₀ = 0.76 μ M), 6 α - and 6 β -haemanthidine (CC₅₀ = 5.43 μ M), 11-hydroxyvittatine (CC₅₀ = 10.57 μ M) and pseudolycorine (CC₅₀ = 3.41 μ M).

Keywords: Amaryllidaceae, DFT calculation, *Pancratium maritimum*, SARS-CoV-2, VCD

1. Introduction

The genus *Pancratium* Dill. ex L. (Amaryllidaceae) consists of approximately 60 plant species according to the World Checklist of Vascular Plants (Govaerts, 2022). The name *Pancratium* is derived from the Greek word “pagkration” which means “almighty”, perhaps due to the medicinal properties that species from this genus possess (Cedrón et al., 2010). *Pancratium maritimum* L. (or ‘sea daffodil’, ‘sea lily’, ‘sand lily’) is widely distributed along the coastline of the Mediterranean region, from the Black Sea to parts of the Atlantic ocean, adapting well to the stressful conditions of sand dune environments (Rhizopoulou and Pouris, 2018). *P. maritimum* has been thoroughly studied and consequently, over half of the alkaloids isolated from the *Pancratium* genus were identified in this plant species (Cedrón et al., 2010). To the best of our knowledge, 42 alkaloids were isolated heretofore from *P. maritimum*, including all known skeleton-types of Amaryllidaceae alkaloids: nine lycorine-types (lycorine, pseudolycorine, hippadine, ungeremine, ungiminoine, ungiminoine *N*-oxide, zefbetaine, α -dihydrocaramine and galanthane), five homolycorine-types (lycorenine, homolycorine, hippeastrine, 8-*O*-demethylhomolycorine and 9-*O*-demethylhomolycorine), four galanthamine-type (galanthamine, *N*-formylnorgalanthamine, habranthine and pancrimatine C), six haemanthamine-types (haemanthamine, two 6-epimers of haemanthidine, 6-*O*-methylhaemanthidine, *O*-demethylhaemanthamine and 8-*O*-demethylmaritidine), five crinine-types (crinine, 3 β ,11 α -dihydroxy-1,2-dehydrocrinane, 8-hydroxy-9-methoxycrinine, crinine-3-one and buphanisine), two tazettine-types (tazettine and 6 α -deoxytazettine), five phenanthridone-types (pancratistatin, narciclasine-4-*O*- β -D-glucopyranoside, *N*-methyl-8,9-methylenedioxy-6-phenanthridone, pancrimatine A and pancrimatine B), two phenanthridine-types (trispheridine and *N*-methyl-8,9-methylenedioxy phenanthridine), one montanine-type (montanine), one norbelladine-type (4'-*O*, *N*-dimethylnorbelladine), and two compounds with a rare scaffold (gralicine and norismine) (Cedrón et al., 2010; Youssef and Frahm, 1998; Ibrahim et al., 2013; Abou-Donia et al., 1992; Berkov et al., 2004; Youssef et al., 2022).

Nowadays, natural product chemists are paying more attention to 3D structure determination for three main reasons: (1) – isomers are a tempting source of undiscovered natural products; (2) – isomers tend to have different biological activities, which is important for discovering potent, novel hits and leads, and (3) – many incorrect stereochemical assignments were reported in the last decades due to over-reliance on conventional spectroscopic tools (NMR, HRMS), which provide insufficient 3D structural information in some cases (Chhetri et al., 2018). Over the past few years, computer-assisted 3D structure elucidation (CASE-3D) has become a powerful tool to support the structural determination process alongside spectroscopic techniques, from 2D to 3D structures, which reduces the occurrence of misassignment (Zanardi et al., 2021; Marcarino et al., 2022). The power of integrating computational calculation into the traditional process of structure elucidation was proven with many recent successful examples (Chhetri et al., 2018; Sarotti, 2020; Le et al.; 2021; Le et al., 2023a). In this study, a re-investigation of the alkaloidal composition of *P. maritimum* resulted in the isolation and complete characterization of eighteen alkaloids, of which one is reported for the first time using the combination of NMR, HRMS and CASE-3D. Furthermore, the absolute configuration of this novel structure was confirmed by means of vibrational circular dichroism (VCD) spectroscopy and infrared (IR) spectroscopy.

Important bioactivities of alkaloids from *P. maritimum* include anticancer, antiplasmodial, anti-inflammatory, antimicrobial and antioxidant activities, which have been explored for decades (Cedrón et al., 2010; Leporini et al., 2018; Cimmino et al., 2017). Antiviral activity of Amaryllidaceae alkaloids also has drawn the attention of many researchers, especially concerning activity against the dengue, HIV and hepatitis viruses (Nair et al., 2023; Masi et al., 2022). Since 2019, the severe acute respiratory syndrome coronavirus-2 (SARS-CoV-2) has emerged, and continues to threaten the well-being of humans. On the one hand, large scale vaccination helped us regain our normal lives, but the goal to permanently eradicate the virus remains challenging, since the virus keeps evolving and new resistant variants keep arising. On the other hand, the use of medicinal plants as complementary and/or alternative medicines still prevails in many places worldwide (Nair et al., 2023; Raman et al., 2022; Christy et al., 2021; Isidoro et al., 2022). However, this practice is primarily based on indigenous and traditional knowledge of plants used for

treating respiratory diseases. In the course of 2020-2022, many natural products were reported to exhibit anti-SARS-CoV-2 activity, originating from various sources (plants, marine sources, microbes) (Avalon et al, 2022; Li et al., 2021). For example, lycorine, the most abundant Amaryllidaceae alkaloid, was named as a potent candidate by several studies (Jin et al., 2021; Ren et al., 2022). Thus, the application of Amaryllidaceae alkaloids for the treatment of SARS-CoV-2 infection became a compelling research topic, not only because of their antiviral potential, but also considering the widespread and highly accessible resources of Amaryllidaceae alkaloids. In the current work, anti-SARS-CoV-2 activity and cytotoxicity were examined for all isolated compounds from *P. maritimum*.

2. Results and discussion

2.1. Structure elucidation of compound 1

The current phytochemical investigation resulted in the isolation and characterization of eighteen alkaloids possessing a wide range of polarities (see **Fig. 1**). Compounds **2, 3, 5, 9, 10, 12 – 15** and **18** were purified from the DCM extract; compounds **1, 4, 6 – 8, 10, 16, 17** from the EtOAc extract. Compound **1** was described in this study for the first time and its structural elucidation process will be elaborated on hereafter. Compound **1** was isolated as white powder (11.0 mg) and compound **2** as yellowish amorphous solid (5.0 mg). Their accurate masses suggested chemical formulas of $C_{17}H_{19}NO_6$ (m/z 334.1290 $[M+H]^+$) and $C_{17}H_{20}NO_4$ (m/z 302.1395 $[M+H]^+$), respectively. Both compounds **1** and **2** possessed a carbon signal at 164.1 ppm (**Table 1**), which was likely to be involved in either a lactone or a lactam ring. In other words, the two plausible Amaryllidaceae scaffolds were either the homolycorine- or the narciclasine-type, respectively. However, due to the presence of a typical N-Me moiety ($\delta_H = 1.82$, $\delta_C = 44.1$) which does not correspond with the NH moiety of the lactam ring of the narciclasine-type, the homolycorine-type scaffold was selected for further NMR analysis. Compared to NMR data of homolycorine reported in the literature, compound **2** only lacked one methoxy group and therefore, based on its 2D NMR spectra, compound **2** was easily assigned as 9-*O*-demethylhomolycorine (Kihara et al., 1991). The molecular weight of compound **1** was 32 mass units higher compared to compound **2**, indicating a possible addition of two oxygens, which

might be due to two additional hydroxy groups. This was confirmed by the ^{13}C NMR data, which revealed that compound **1** indeed possessed two more oxygenated carbons (occurring around 70 ppm in ^{13}C NMR) than compound **2**.

Next, separate moieties were elucidated by HSQC and COSY correlations prior to connecting them. Two methylene signals were observed in the HSQC spectrum: $\delta_{\text{H}}\text{-}3.05/\delta_{\text{H}}\text{-}2.21$ and $\delta_{\text{H}}\text{-}2.44/\delta_{\text{H}}\text{-}2.38$. They also correlated with each other in the COSY spectrum (**Fig. 2**). Another spin system was identified by COSY cross-peaks between $\delta_{\text{H}}\text{-}5.57$, $\delta_{\text{H}}\text{-}4.10$ and $\delta_{\text{H}}\text{-}4.35$, and the three hydrogens were all methine groups. Two singlets, occurring at 7.16 and 7.31 ppm, must belong to the aromatic ring. An N-Me, as aforementioned, and an O-Me ($\delta_{\text{H}} = 3.82$, $\delta_{\text{C}} = 56.1$) were also identified (**Table 1**).

Starting from the benzene ring, it is known for the homolycorine-type skeleton that due to the presence of a lactone moiety, the signal of H-7 is more downfield than the one corresponding to H-10. Thus, $\delta_{\text{H}}\text{-}7.31$ was assigned to H-7 and $\delta_{\text{H}}\text{-}7.16$ to H-10. The HMBC correlation between $\delta_{\text{H}}\text{-}7.31$ and $\delta_{\text{C}}\text{-}164.1$ further confirmed the assignment (**Fig. 2**). Attachment of the O-Me group to the benzene ring was deduced from the HMBC correlation between $\delta_{\text{H}}\text{-}3.82$ and $\delta_{\text{C}}\text{-}147.9$, and the NOESY cross-peak between $\delta_{\text{H}}\text{-}3.82$ and $\delta_{\text{H}}\text{-}7.31$ (H-7) proved its position at C-8. The NOE effect observed between H-10 and N-Me again confirmed a homolycorine-type skeleton, since only this subclass can provide spatial proximity between these hydrogens. Compared to compound **2**, an exact match was found for the NMR data of the nitrogen-containing ring, implying that this moiety was also present in compound **1** (C-4, C-4a, C-11 and C-12). Therefore, it was obvious that the main structural discrepancies should be found in the two rings in the middle of the homolycorine scaffold. The olefinic hydrogen and carbon ($\delta_{\text{H}}\text{-}5.57$ and $\delta_{\text{C}}\text{-}119.6$) were also similar to compound **2**. Given the fact that compound **2** has a four-membered spin system formed by three methine groups and a methylene, and that compound **1** has a three-membered spin system formed by three methine groups, the two additional hydroxy groups must be located at C-10b and C-2 (**Fig. 2**). Combining all data, the structure of compound **1** was proposed as shown in Figures 1 and 3. In 2015, Carvalho et al. reported 2 α -10b α -dihydroxy-9-*O*-demethylhomolycorine possessing the same 2D structure, but H-4a of this compound was found at 4.24 ppm in ^1H -NMR, while that of compound **1** was 2.60 ppm (Kaline et al.,

2015). Hence, compound **1** must be a diastereomer of the reported compound and was characterized for the first time.

As the NOESY experiment did not provide sufficient information to deduce the relative configuration of compound **1**, ^1H and ^{13}C chemical shifts were computed to perform DP4 and DP4+ probabilistic methods (**Table 1**). **Table 2** displays the probabilities of eight possible diastereomers, and in fact both DP4 and DP4+ led to an identical result (the RRRR configuration). As shown in Table 1, the root-mean-square-deviations (RMSD) obtained were maximum 2.0 ppm for carbons and 0.15 ppm for hydrogens, which is considered as a perfect match between experimental and calculated values. The maximum outlier observed (E_{max}) was that of C-11, but C-11 is not a stereocenter and is located two bonds away from the nearest stereocenter (C-4a); therefore, it does not significantly contribute to the stereochemical information. After combining all ^1H and ^{13}C data, the relative configuration (1*R*, 2*R*, 4*aR*, 10*bR*) which possesses a probability of 100% was proposed for compound **1**. VCD analysis was performed to verify the propositions from DP4 and DP4+ probabilities (**Fig. 3**). Experimental VCD and IR spectra were measured in $(\text{CD}_3)_2\text{SO}$. A careful analysis of the experimental data and the results obtained with the DFT calculations was performed, with attention for the robustness of the calculated spectra (see Supporting Information). From this, it became clear that RRRR matches best to the experimental spectrum (compared to SSSS). Therefore, the absolute configuration of compound **1** was confirmed to be (1*R*, 2*R*, 4*aR*, 10*bR*), and the name 2 β ,10*b* α -dihydroxy-9-*O*-demethylhomolycorine was adopted.

NMR data of compounds **3** – **18** matched with those of compounds reported in literature and were identified as galanthamine (**3**) (Zotta et al., 1971), habranthine (**4**) (Wildman et al., 1968), haemanthamine (**5**) (Zotta et al., 1971), 6 α -haemanthidine (**6**) and 6 β -haemanthidine (**7**) (Zhang et al., 2006), 11-hydroxyvittatine (**8**) and vittatine (**9**) (Viladomat et al., 1995), lycorine (**10**), pseudolycorine (**11**), 1-*O*-acetyl-norpluviine (**12**) (Campbell et al., 2000), 1-*O*-acetyl-10-*O*-methylpseudolycorine (**13**) (Sarıkaya et al., 2013), unginorine (**14**) (Richomme et al., 1989), unginorine *N*-oxide (**15**) and ungeremine (**16**) (Suau et al., 1988), narciclasine (**17**) (Southgate et al., 2017), and 4'-*O*-methylnorbelladine (**18**) (Ghosal et al., 1985). Among those, three compounds, i.e. 1-*O*-acetyl-norpluviine, 1-*O*-acetyl-10-*O*-methylpseudolycorine and 4'-*O*-

methylnorbelladine were isolated from *P. maritimum* for the first time. Detailed experimental NMR and MS data can be found as Supporting Information.

2.2. Anti-SARS-CoV-2 activity and cytotoxicity

All analogues were evaluated for antiviral activity in SARS-CoV-2 infected VeroE6 cells. GS-441524, the parent nucleoside of remdesivir was included as positive control, displaying an EC₅₀ value of 0.81 μM and a CC₅₀ value of 72.38 μM. 9-*O*-demethylhomolycorine (**2**), galanthamine (**3**), 1-*O*-acetyl-norpluviine (**12**), and 1-*O*-acetyl-10-*O*-methylpseudolycorine (**13**) exhibited weak inhibition of SARS-CoV-2 (EC₅₀ = 44-80 μM) at non-cytotoxic concentrations (CC₅₀ > 100 μM). 9-*O*-Demethylhomolycorine (**2**) and 1-*O*-acetyl-10-*O*-methylpseudolycorine (**13**) were the most potent ones among all tested compounds, both displaying EC₅₀ values of around 45 μM in duplicate, respectively. Habranthine (**4**), unginorine (**14**), unginorine *N*-oxide (**15**), ungeremine (**16**), and 4'-*O*-methylnorbelladine (**18**) were devoid of activity and cytotoxicity. The cytotoxicity of lycorine (**10**) on a Vero E6 cell line was previously reported by the authors in two studies of alkaloids isolated from *Hymenocallis littoralis* and *Scadoxus multiflorus* (Le et al., 2023b; Le et al. 2023c). Apart from them, it was observed in the current investigation, using the same assay, that 2β,10β-dihydroxy-9-*O*-demethylhomolycorine (**1**), haemanthamine (**5**), 6α- and 6β-haemanthidine (**6** and **7**), 11-hydroxyvittatine (**8**), and pseudolycorine (**11**) lacked selective antiviral activity, since they were cytotoxic to the Vero E6 cells as evidenced by CC₅₀ values of 13.28 μM, 0.76 μM, 5.43 μM, 10.57 μM, and 3.41 μM, respectively.

3. Conclusion

In this study, a re-investigation of the alkaloidal composition of *P. maritimum* led to the isolation of an undescribed alkaloid (2β,10β-dihydroxy-9-*O*-demethylhomolycorine) and 17 known ones. Three compounds (1-*O*-acetyl-norpluviine, 1-*O*-acetyl-10-*O*-methylpseudolycorine and 4'-*O*-methylnorbelladine) were isolated from *P. maritimum* for the first time. Assessment of anti-SARS-CoV-2 activity and cytotoxicity on a Vero E6 cell line revealed four compounds with weak anti-SARS-CoV-2 potency at non-cytotoxic concentrations, namely of 9-*O*-demethylhomolycorine (**2**), galanthamine (**3**), 1-

O-acetyl-norpluviine (**12**), and 1-*O*-acetyl-10-*O*-methylpseudolycorine (**13**) with EC₅₀ values of 44 μM, 70 μM, 80 μM, and 47 μM, respectively. Cytotoxicity was observed for 2β,10β-dihydroxy-9-*O*-demethylhomolycorine (**1**) (CC₅₀ = 13.28 μM), haemanthamine (**5**) (CC₅₀ = 0.76 μM), 6α- and 6β-haemanthidine (**6** and **7**) (CC₅₀ = 5.43 μM), 11-hydroxyvittatine (**8**) (CC₅₀ = 10.57 μM), and pseudolycorine (**11**) (CC₅₀ = 3.41 μM). Although only weak anti-SARS-CoV-2 activity was observed in the VeroE6 cells for a selected number of derivatives, it might be worthwhile to evaluate their anti-SARS-CoV-2 activity in physiologically more relevant cell types, such as in the lung cancer cell lines Calu-3 and A549.

4. Material and Methods

4.1. General experimental procedures

Analytical grade solvents, including methanol, ethanol, ethyl acetate and dichloromethane were purchased from Acros Organics (Geel, Belgium) or from Fisher Scientific (Loughborough, UK). Reagents, including TLC spraying reagents: ammonia 25% (NH₄OH 25%), formic acid (FA 98%), MS-grade formic acid (FA 99%), hydrochloric acid 25% (HCl 25%), potassium iodide (KI 99%) and bismuth (III) nitrate (Bi(NO₃)₃ 99.5%) were purchased from either Acros Organics (Geel, Belgium), Sigma-Aldrich (St. Louis, MO, USA) or Merck (Darmstadt, Germany). Solvents used for HPLC and UPLC, i.e. methanol (MeOH) and acetonitrile (ACN) were HPLC and UPLC grade and were purchased from Fisher Scientific (Loughborough, UK) and Biosolve BV (Valkenswaard, the Netherlands), respectively. Milli-Q water was obtained by filtering RO water by a Direct-Pure Up Ultrapure system (Rephile Bioscience, Belgium). For NMR experiments, methanol-*d*₄ (CD₃OD - 99.8% D), chloroform-*d* (CDCl₃ - 99.8% D) and dimethyl sulfoxide-*d*₆ (99.9% D) were purchased from Sigma-Aldrich (Merck, Germany).

TLC was performed on pre-coated silica gel F254 plates (Merck, Darmstadt, Germany). After developing TLC, the bands were observed under UV light (254 and 366 nm), as well as under visible light after spraying with the Dragendorff reagent.

Flash chromatography was performed on a Grace Reveleris X2 system (Columbia, MD, USA) using the Reveleris Navigator™ software. The system consists of a binary pump, a UV detector, an evaporative light scattering detector and a fraction collector.

An Agilent 1200 series HPLC-DAD system (Agilent Technologies, Santa Clara, USA) with OpenLAB software version A.01.05, operated with a Phenomenex Kinetex EVO C18 column (250 x 4.6 mm, 5 µm) was used for all HPLC analyses. For purification, a preparative HPLC-DAD-MS system was used. All its compartments were supplied by Waters (Milford, MA, USA), including MassLynx v.4.1 software. A Phenomenex Kinetex EVO C18 column (250 x 10.0 mm, 5 µm) was selected for the semi-preparative separation (Phenomenex, Utrecht, the Netherlands).

NMR spectra were recorded either on a DRX-400 or an Avance Nanobay III NMR instrument (Bruker BioSpin, Rheinstetten, Germany), both operating at 400 MHz for ¹H and 100 MHz for ¹³C analysis. NMR data processing was performed using TopSpin software version 4.0.6 from Bruker.

Accurate mass-to-charge measurements were conducted on a UPLC-QTOF-MS/MS (Xevo G2-XS QTOF mass spectrometer), comprising an Acquity UPLC (Waters Corporation, Milford, MA, USA) and using MassLynx software version 4.1. A BEH C18 column (100 x 2.1 mm, 1.7 µm, Waters) was used. Optical rotations were measured on a Jasco P-2000 spectropolarimeter (Easton, MD, USA) equipped with the Spectra Manager™ software.

4.2. Plant material

About 4 kg of fresh bulbs of *P. maritimum* were collected between April and June 2017 in ‘Praia do Ancão’, Southern Portugal (Algarve, Loulé), GPS coordinates 37°01'59.4"N 8°02'15.4"W. A voucher specimen (no. MBH37), identified by Dr. Luisa Custodio, is kept at the Centre of Marine Sciences, University of Algarve, Faro, Portugal. Freeze-drying yielded about 750 g of residue.

4.3. Extraction and isolation

Ultrasonication-assisted extraction with methanol was carried out on roughly 700 g of freeze-dried material (2.5 L x 5). After evaporating solvent under reduced pressure, 80 g of crude extract was obtained and subsequently suspended in water. The general alkaloidal extraction procedure was then applied. Briefly,

the water suspension was acidified to pH < 3 by HCl 5%, following by liquid-liquid partitioning with DCM (x3) to remove acidic impurities. Next, the water phase was basified to pH > 9 by NH₄OH 25% before partitioning with DCM (x3) which yielded the first alkaloid extract (4.4 g DCM extract). The third liquid-liquid partition with EtOAc (x3) was performed thereafter yielding 2.0 g EtOAc extract.

The two extracts were further fractionated by flash chromatography using the solvent mixture of DCM and MeOH + 0.5% NH₄OH and normal phase silica gel. As for the DCM extract, the following gradient was used: 0-10 min (0% MeOH), 10-20 min (5% MeOH), 20-35 min (10% MeOH), 35-45 min (20% MeOH), 45-55 min (30% MeOH), 55-65 min (40% MeOH), 65-80 min (80% MeOH); while the gradient was halted during elution of detected compounds. The gradient applied to the EtOAc extract was as follows: 0-5 min (0% MeOH), 5-10 min (5% MeOH), 10-20 min (10% MeOH), 20-30 min (20% MeOH), 30-40 min (30% MeOH), 50-60 min (40% MeOH), 60-70 min (50% MeOH), 70-80 min (80% MeOH). In the end, 22 fractions were obtained from the DCM extract (DCM-1 to DCM-22), and 26 fractions from the EtOAc extract (EtOAc-1 to EtOAc-22).

Lycorine (**10**) crystallized directly in many fractions as white needles and was washed with methanol to remove it before all fractions were subjected to analytical HPLC. After profiling, promising fractions were selected for semi-preparative separation.

Semi-preparative HPLC-DAD-MS with manual collection was performed for isolation of pure compounds from the fractions DCM-3, DCM-4, DCM-8, DCM-12, DCM-13, EtOAc-6, EtOAc-7, and EtOAc-15. More specifically, the general preparative LC conditions for all fractions were: (1) sample concentration: 1 mg/mL in water; (2) injection volume: 200 - 600 μ L; (3) solvent A: H₂O + 0.5% NH₄OH and solvent B: MeOH + 0.5% NH₄OH; (4) UV detection: 210 and 254 nm; (6) flow rate: 3 mL/min. Compounds **2**, **12**, **13**, **18** were purified from fractions DCM-3 and DCM-4; compounds **12** – **15** from DCM-8; compounds **3**, **5**, **9**, **10** from DCM-12 and DCM-13; compounds **1**, **4**, **6** – **8** from EtOAc-6 and EtOAc-7; and compounds **10**, **16**, **17** from EtOAc-15.

2 β ,10 α -dihydroxy-9-*O*-demethylhomolycorine (**1**)

White powder (11.0 mg); UV λ_{\max} 210, 254 nm; ^1H - and ^{13}C -NMR ($(\text{CD}_3)_2\text{SO}$, 400 and 100 MHz): see Table 1; Positive HRESIMS m/z 334.1290 $[\text{M}+\text{H}]^+$ (calcd for $\text{C}_{17}\text{H}_{20}\text{NO}_6$, 334.1291)

4.4. Computational methods

Conformational analysis was performed by PCMODEL (version 10.0) using the MMFF94 force field applying 8 and 7 kcal.mol⁻¹ energy windows for two consecutive conformational search cycles. Afterwards, for chemical shift calculations, the level PCM/mPW1PW91/6-311G**//M06-2X/6-31G** was applied for DP4 probability and the level PCM/mPW1PW91/6-311G+(d,p)//B3LYP/6-31G* for DP4+ probability. After dereplication, resulting isotropic shielding values were referenced to TMS and then either scaled by linear regression for DP4 probability or used directly for DP4+ probability. To compute VCD and IR spectra, the level PCM/B3LYP/6-311G++(2d,2p) was chosen. PCM solvation model was carried out with $(\text{CD}_3)_2\text{SO}$ to mimic experimental conditions.

Geometry optimization, frequency and shielding tensor quantum mechanical calculations were performed by the Gaussian16 program. Boltzmann distribution was estimated using the sum of electronic and thermal free energies at 298.15 K. Only conformers having energies within 2.5 kcal mol⁻¹ from the global minimum were considered as contributing ones and submitted to the GIAO (Gauge-Independent Atomic Orbital) and VCD simulations.

4.5. Anti-SARS-CoV-2 assay

The SARS-CoV-2 antiviral assay is based on a previously described SARS-CoV-1 assay and has been described before by us (Ivens et al., 2005; Le et al. 2023b). Briefly, on day -1, the test compounds were serially diluted in assay medium (DMEM supplemented with 2% v/v FCS). The plates were incubated (37 °C, 5% CO₂ and 95% relative humidity) overnight. On day 0, the diluted compounds were then mixed with SARS-CoV-2 at 20 TCID₅₀/well and VeroE6-eGFP cells corresponding to a final density of 25,000 cells/well in 96-well blackview plates (Greiner Bio-One, Vilvoorde, Belgium; Catalog 655090). The plates were incubated in a humidified incubator at 37 °C and 5% CO₂. At 4 days p.i., the wells were examined for eGFP expression using an argon laser-scanning microscope. The microscope settings were excitation at 488

nm and emission at 510 nm and the fluorescence images of the wells were converted into signal values. The results were expressed as EC₅₀ values defined as the concentration of compound achieving 50% inhibition of the virus-reduced eGFP signals as compared to the untreated virus-infected control cells. Toxicity of compounds in the absence of virus was evaluated in a standard MTS-assay as reported previously (Jochmans et al., 2012).

Declaration of competing interest

The authors declare no conflicts of interest.

Acknowledgments

M. Theunis, K. Foubert and T. Naessens are acknowledged for their immense help with the analytical instruments. The computational resources used in this work were provided by the HPC core facility CalcUA of the University of Antwerp, and VSC (Flemish Supercomputer Center), funded by the Research Foundation - Flanders (FWO) and the Flemish Government. The SARS-CoV-2 screening was performed using the 'Caps-It' research infrastructure (project ZW13-02) that was financially supported by the Hercules Foundation (Research Foundation - Flanders) and Rega Foundation, KU Leuven. The Research Foundation - Flanders is also acknowledged for financial support (research project G014521N).

Author contribution

N. T. H. L.: isolation, structure elucidation and writing the manuscript; S. D. J., K. E., C. P., J. N.: assessment of antiviral activity; T. V.: VCD and optical rotation measurement; W. A. H., L. P., E. T.: conceptualization, discussion and writing the manuscript.

Appendix A. Supplementary data

HRMS and NMR spectra of compound **1**, ¹H and ¹³C NMR data of compounds **2–18**, computed VCD and IR of all configurations, contributing conformers for DFT calculation and detailed anti-SARS-CoV-2 results are available as Supporting Information.

References

- Abou-Donia AH, Abib A-A, El Din AS, Evidente A, Gaber M, Scopa A, 1992. Two betaine-type alkaloids from Egyptian *Pancreatium maritimum*. *Phytochemistry*. 31, 2139–2141
- Avalon NE, Nafie J, De Marco Verissimo C, Warrensford LC, Dietrick SG, Pittman AR, Young RM, Kearns FL, Smalley T, Binning JM, Dalton JP, Johnson MP, Woodcock HL, Allcock AL, Baker BJ, 2022. Tuaimenal A, a meroterpene from the Irish deep-sea soft coral *Duba floridana*, displays inhibition of the SARS-CoV-2 3CLpro enzyme. *J. Nat. Prod.* 85, 1315–1323
- Berkov S, Evstatieva L, Popov S, 2004. Alkaloids in Bulgarian *Pancreatium maritimum* L. *Zeitschrift für Naturforsch C*. 59, 65–69
- Campbell WE, Nair JJ, Gammon DW, Codina C, Bastida J, Viladomat F, Smith PJ, Albrecht CF, 2000. Bioactive alkaloids from *Brunsvigia radulosa*. *Phytochemistry*. 53, 587–591
- Cedrón JC, Del Arco-Aguilar M, Estévez-Braun A, Ravelo ÁG, 2010. Chemistry and biology of *Pancreatium* Alkaloids. *Alkaloids Chem. Biol.* 68, 1–37
- Chhetri BK, Lavoie S, Sweeney-Jones AM, Kubanek J, 2018. Recent trends in the structural revision of natural products. *Nat. Prod. Rep.* 35, 514–531
- Christy MP, Uekusa Y, Gerwick L, Gerwick WH, 2021. Natural products with potential to treat RNA virus pathogens including SARS-CoV-2. *J. Nat. Prod.* 84, 161–182
- Cimmino A, Masi M, Evidente M, Superchi S, Evidente A, 2017. Amaryllidaceae alkaloids: Absolute configuration and biological activity. *Chirality*. 29, 486–499
- De Castro O, Di Maio A, Di Febraro M, Imperato G, Innangi M, Vela E, Menale B, 2016. A multi-faceted approach to analyse the effects of environmental variables on geographic range and genetic structure of a perennial psammophilous geophyte: The case of the sea daffodil *Pancreatium maritimum* L. in the mediterranean basin. *PLoS One*. 11, 1–23
- Ghosal S, S. Saini K, Razdan S, 1985. Crinum alkaloids: their chemistry and biology. *Phytochemistry*. 24, 2141–2156
- Govaerts R, 2022. The World Checklist of Vascular Plants (WCVP). *R. Bot. Gard.*
- Ibrahim SRM, Mohamed GA, Shaala LA, Youssef DTA, El Sayed KA, 2013. New alkaloids from *Pancreatium maritimum*. *Planta. Med.* 79, 1480–1484
- Ivens T, Van Den Eynde C, Van Acker K, Nijs E, Dams G, Bettens E, Ohagen A, Pauwels R, Hertogs K, 2005. Development of a homogeneous screening assay for automated detection of antiviral agents active against severe acute respiratory syndrome-associated coronavirus. *J. Virol. Methods*. 129, 56–63
- Isidoro C, Chiung-Fang Chang A, Sheen LY, 2022. Natural products as a source of novel drugs for treating

- SARS-CoV2 infection. J. Tradit. Complement. Med. 12, 1–5
- Jin YH, Min JS, Jeon S, Lee J, Kim S, Park T, Park D, Jang MS, Park CM, Song JH, Kim HR, Kwon S, 2021. Lycorine, a non-nucleoside RNA dependent RNA polymerase inhibitor, as potential treatment for emerging coronavirus infections. *Phytomedicine*. 86, 153440
- Jochmans D, Leyssen P, Neyts J, 2012. A novel method for high-throughput screening to quantify antiviral activity against viruses that induce limited CPE. *J. Virol. Methods*. 183, 176–179
- Kihara M, Konishi K, Xu L, Kobayashi S, 1991. Alkaloidal constituents of the flowers of *Lycoris radiata* HERB. (Amaryllidaceae). *Jstage*. 39, 1849–1853
- Kaline R. Carvalho ABS, Maria Conceição M. Torres FCLP, Larissa A. Guimarães DDR, Edilberto R. Silveira LVC-L, Raimundo Braz-Filho and Oflia Deusdênia. L. Pessoa, 2015. Cytotoxic alkaloids from *Hippeastrum solandriflorum* Lindl. *J. Braz. Chem. Soc*. 26, 1976–1980
- Le HTN, Van Roy E, Dendooven E, Peeters L, Theunis M, Foubert K, Pieters L, Tuenter E, 2021. Alkaloids from *Lepidium meyenii* (Maca), structural revision of macaridine and UPLC-MS/MS feature-based molecular networking. *Phytochemistry*. 190, 112863
- Le NTH, Vermeyen T, Aerts R, Herrebout A W, Pieters L, Tuenter E, 2023a. Epimeric mixture analysis and absolute configuration determination using an integrated spectroscopic and computational approach – a case study of two epimers of 6-hydroxyhippeastidine. *Molecules*. 28(1), 214
- Le NTH, De Jonghe S, Erven K, Neyts J, Pannecouque C, Vermeyen T, Herrebout A W, Pieters L, Tuenter E, 2023b. Anti-SARS-CoV-2 activity and cytotoxicity of Amaryllidaceae alkaloids from *Hymenocallis littoralis*. *Molecules*. 28(7), 3222
- Le, NTH, De Jonghe, S., Erven, K., Neyts, J., Pannecouque, C., Vermeyen, T., Herrebout A W, Pieters L, Tuenter, E. (2023c). Comprehensive study of alkaloids from *Scadoxus multiflorus* by HPLC-PDA-SPE-NMR and evaluation of their anti-SARS-CoV-2 activity. *Phytochemistry letters*, 57, 156-162.
- Leporini M, Catinella G, Bruno M, Falco T, Tundis R, Loizzo MR, 2018. Investigating the antiproliferative and antioxidant properties of *Pancreatum maritimum* L. (Amaryllidaceae) stems, flowers, bulbs, and fruits extracts. *Evidence-based Complement. Altern. Med*. 2018
- Li YT, Yang C, Wu Y, Lv JJ, Feng X, Tian X, Zhou Z, Pan X, Liu S, Tian LW, 2021. Axial chiral Binaphthoquinone and Perylenequinones from the stromata of *Hypocrella bambusae* are SARS-CoV-2 entry inhibitors. *J. Nat. Prod*. 84, 436–443
- Marcarino MO, Cicetti S, Zanardi MM, Sarotti AM, 2022. A critical review on the use of DP4+ in the structural elucidation of natural products: the good, the bad and the ugly. A practical guide. *Nat. Prod. Rep*. 39, 58–76
- Nair JJ, van Staden J, 2023. Antiviral alkaloid principles of the plant family Amaryllidaceae. *Phytomedicine*. 108, 154480

- Masi M, Di Lecce R, Mérendol N, Girard M-P, Berthoux L, Desgagné-Penix I, Calabrò V, Evidente A, 2022. Cytotoxicity and antiviral properties of alkaloids isolated from *Pancreatium maritimum*. *Toxins* (Basel). 14, 262
- Raman K, Rajagopal K, Islam F, Dhawan M, Mitra S, Aparna B, Varakumar P, Byran G, Choudhary OP, Emran T Bin, 2022. Role of natural products towards the SARS-CoV-2: A critical review. *Ann Med Surg.* 80, 104062
- Ren P xuan, Shang W juan, Yin W chao, Ge H, Wang L, Zhang X lei, Li B qian, Li H lin, Xu Y chun, Xu EH, Jiang H liang, Zhu L li, Zhang L ke, Bai F, 2022. A multi-targeting drug design strategy for identifying potent anti-SARS-CoV-2 inhibitors. *Acta. Pharmacol. Sin.* 43, 483–493
- Rhizopoulou S, Pouris J, 2018. On *Pancreatium maritimum* (sea daffodil, sea lily, sand lily). *Hortic Int Journal.* 2, 116–118
- Richomme P, Pabuccuoglu V, Gozler T, Freyer A, Shamma M, 1989. (-)-siculinine: a lycorine-type alkaloid from *Sternbergia sicula*. 52, 1150–1152
- Sarotti AM, 2020. In Silico Reassignment of (+)-Diplopyrone by NMR calculations: use of a DP4/ J-DP4/DIP tandem to revise both relative and absolute configuration. *J. Org. Chem.* 85, 11566–11570
- Sarikaya BB, Kaya GI, Onur MA, Bastida J, Somer NU, 2013. Phytochemical investigation of *Galanthus woronowii*. *Biochem. Syst. Ecol.* 51, 276–279
- Southgate EH, Holycross DR, Sarlah D, 2017. Total synthesis of Lycoricidine and Narciclasine by chemical dearomatization of bromobenzene. *Angew. Chemie – Int. Ed.* 56, 15049–15052
- Suau R, Gómez AI, Rico R, Tato MPV, Castedo L, Riguera R, 1988. Alkaloid N-oxides of amaryllidaceae. *Phytochemistry.* 27, 3285–3287
- Wildman WC, Brown CL, 1968. The structure of habranthine. *Tetrahedron Lett.* 9, 4573–4576
- Viladomat F, Bastida J, Codina C, Campbell WE, Mathee S, 1995. Alkaloids from *Boophane flava*. *Phytochemistry.* 40, 307–311
- Youssef DTA, Frahm AW, 1998. Alkaloids of the flowers of *Pancreatium maritimum*. *Planta. Med.* 64, 669–670
- Youssef DTA, Shaala LA, Altyar AE, 2022. Cytotoxic phenylpropanoid derivatives and alkaloids from the flowers of *Pancreatium maritimum* L. *Plants.* 11, 1–13
- Zanardi MM, Sarotti AM, 2021. Sensitivity Analysis of DP4+ with the probability distribution terms: development of a universal and customizable Method. *J. Org. Chem.* 86: 8544–8548
- Zotta BL, Gatti G, Fuganti C, 1971. ¹³C nuclear magnetic resonance spectra of Amaryllidaceae alkaloids. 1–5
- Zhang FM, Tu YQ, Liu JD, Fan XH, Shi L, Hu XD, Wang SH, Zhang YQ, 2006. A general approach to

crinine-type Amaryllidaceae alkaloids: total syntheses of (±)-haemanthidine, (±)-pretazettine, (±)-tazettine, and (±)-crinamine. *Tetrahedron*. 62, 9446–9455

Legends of figures

Fig. 1. Structures of 18 isolated alkaloids from *Pancreatum maritimum*

Fig. 2. Key COSY, HMBC and NOESY correlations observed in compound **1**

Fig. 3. Experimental and calculated VCD of 2 β ,10 α -dihydroxy-9-*O*-demethylhomolycorine (**1**)

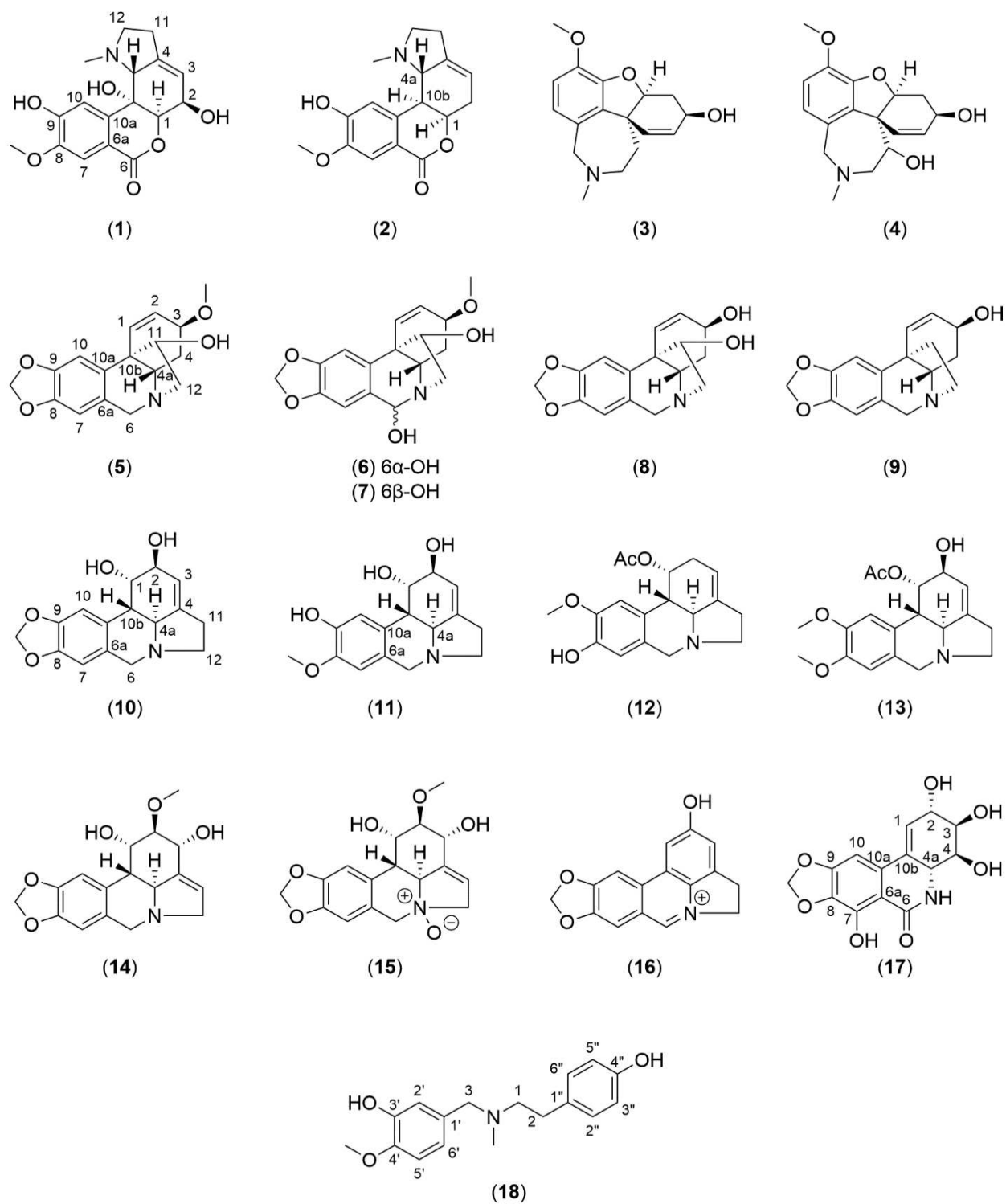


Fig. 1. Structures of 18 isolated alkaloids from *Pancratium maritimum*

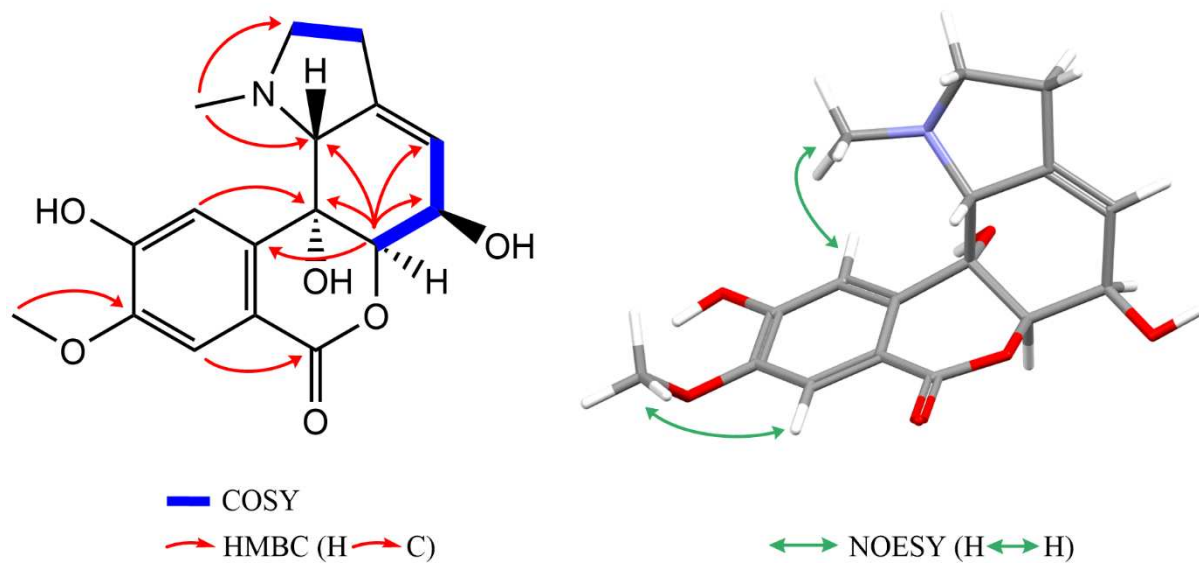


Fig. 2. Key COSY, HMBC and NOESY correlations observed in compound 1

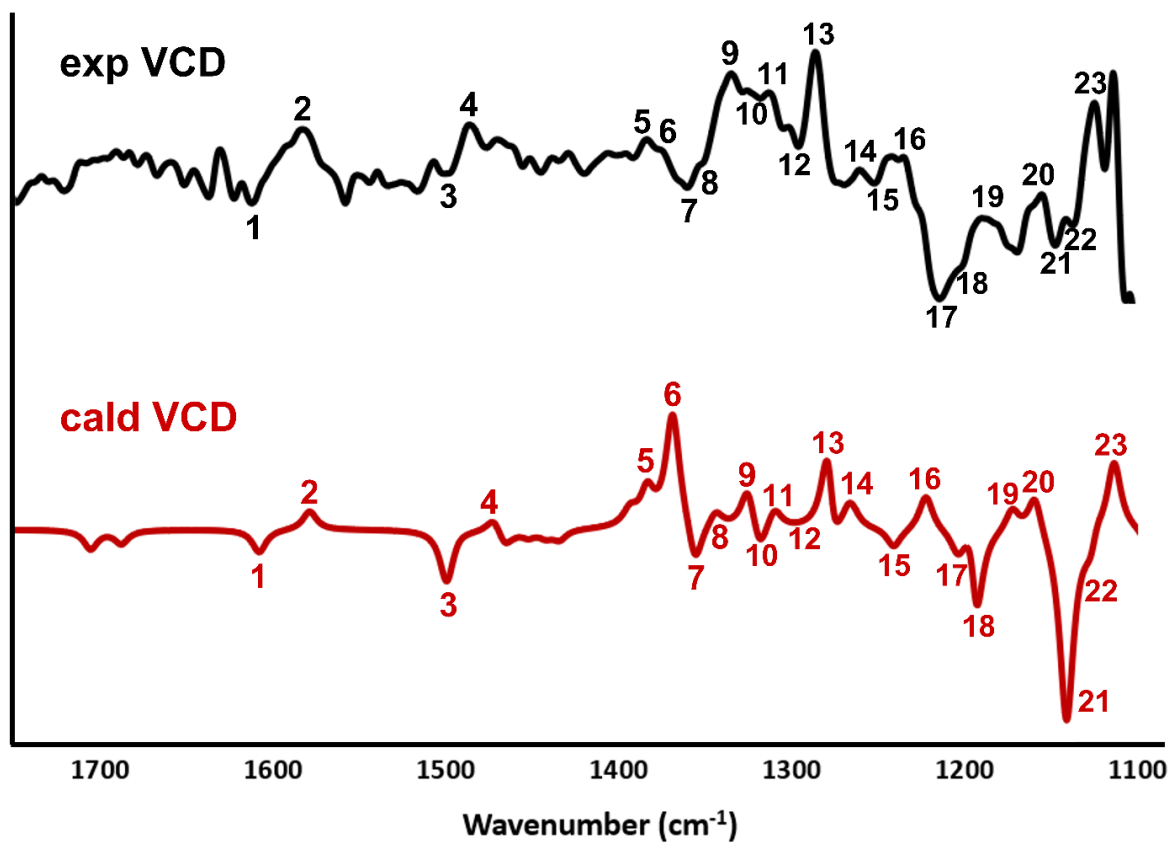


Fig. 3. Experimental and calculated VCD of 2 β ,10 α -dihydroxy-9-*O*-demethylhomolycorine (1)

Table 1. Experimental and calculated ^1H and ^{13}C -NMR data of compound **1** in $(\text{CD}_3)_2\text{SO}$

Position	Experimental		DP4		DP4+	
	δ_{H} (mult., J in Hz)	δ_{C}	δ_{H}	δ_{C}	δ_{H}	δ_{C}
1	4.35 (s)	83.9	4.47	81.1	4.26	80.8
2	4.1*	68.0	4.35	67.1	4.23	66.8
3	5.57 (m)	119.6	5.68	122.6	5.63	122.7
4		142.5		145.4		145.4
4a	2.6 (brs)	70.2	3.01	69.3	2.93	69.3
6		164.1		163.8		163.7
6a		113.6		114.7		114.6
7	7.31 (s)	112.3	7.35	111.5	7.42	111.8
8		147.9		145.1		145.3
9		152.2		151.6		151.6
10	7.16 (s)	112.7	7.07	110.0	7.12	110.2
10a		142.5		144.8		144.6
10b		67.9		71.1		70.6
11	2.38*	28.4	1.95	32.8	1.97	32.6
	2.44*	28.4	2.40	32.8	2.46	32.6
12	2.21 (q, 8.7)	56.0	2.40	55.0	2.38	55.1
	3.05 (td, 8.6, 3.4)	56.0	2.93	55.0	2.95	55.1
N-Me	1.82 (s)	44.1	1.85	42.4	1.87	42.6
8-OMe	3.82 (s)	56.1	3.65	53.7	3.70	54.1
2-OH	4.80 (d, 7.2)					
10b-OH	4.96 (brs)					
9-OH	10.3 (brs)					
RMSD			0.15	2.0	0.12	1.9
E_{Max}			0.43	4.4	0.41	4.2

**overlapping signals*

Table 2. DP4 and DP4+ probabilities (%). Stereocenter order is (1, 2, 4a, 10b).

Diastereomer	DP4			DP4+		
	¹ H	¹³ C	¹ H and ¹³ C	¹ H	¹³ C	¹ H and ¹³ C
RRRR	99.89	4.06	100.00	8.26	0.02	100.00
RRRS	0.00	0.08	0.00	0.00	0.00	0.00
RRSR	0.00	0.01	0.00	0.00	0.00	0.00
RRSS	0.00	0.06	0.00	0.00	0.00	0.00
RSRR	0.00	95.64	0.00	0.00	99.98	0.00
RSRS	0.00	0.12	0.00	0.00	0.00	0.00
RSSR	0.11	0.00	0.00	91.74	0.00	0.00
RSSS	0.00	0.03	0.00	0.00	0.00	0.00